SUPPLEMENTARY MATERIALS FOR:

Pressures of skarn mineralization at Casting Copper, Nevada, based on apatite inclusions in garnet

Drew W. Barkoff[1], Kyle T. Ashley[2†], and Matthew Steele-MacInnis[1*]

[1]Dept. of Geosciences, The University of Arizona, 1040 E. 4th Street, Tucson, AZ 85721 USA

[2]Jackson School of Geosciences, Department of Geological Sciences, University of Texas at Austin, 2305 Speedway Stop C1160, Austin, TX 78712 USA

[*]Current address: Department of Earth and Atmospheric Sciences, The University of Alberta, Edmonton, Alberta T6G 2E3, Canada. Email: steelema@ualberta.ca

[†]Current address: Department of Geology and Environmental Science, University of Pittsburgh, 4107 O'Hara St., Pittsburgh, PA 15260, USA

Supplementary Methods

Unpolarized Raman spectra were collected using a Thermo Nikolet Almega microRaman system at the Mike Scott Laboratory for Mineralogy and Crystallography at the University of Arizona. Raman spectra were collected in a back-scattering arrangement. We used a 532 nm excitation laser, with laser power set to ~100mW. Focusing of the excitation laser onto the apatite inclusions was accomplished using a Nikon 10x, long working distance objective on an Olympus BX51 microscope. The spectrometer position was calibrated using the ca. 1100 cm^{-1} Raman line of sparry calcite. Raman spectra were analyzed using the PeakFit v.4.11 software package from SYSTAT Software Inc.

Inclusion *P* for fluorapatite inclusions at room *T* were determined through the *P*-sensitive frequency shift of the 964 cm^{-1} band. The equation for the relationship at 25°C, calculated with the experimental data of Schouwink *et al.,* (2010), is

$$P(MPa) = \frac{(a*\Delta\nu^2)+(b*\Delta\nu)}{1000} \quad \text{eq. 1}$$

where *a* and *b* are regression parameters equal to 7.35 ± 1.88 and 2265 ± 59, respectively. The Δν term is the difference between the measured peak position of a pressurized inclusion and the reference (0.1 MPa) peak position, at 25°C.

Formation *P* is calculated using the elastic model by Guiraud and Powell, (2006), with a simple linear-mixing correction for garnet and apatite compositions on the resultant *P* calculations. The *P*-*T* conditions that correspond to a particular inclusion *P* (P_{inc}) can be determined using

$$\frac{V_h(P,T)}{V_h(P_0,T_0)} = \frac{V_i(P_i,T)}{V_i(P_0,T_0)} - \frac{3}{4G}(P_i - P) \quad \text{eq. 2}$$

where *G* is the shear modulus of the host mineral. Elastic and volumetric parameters for apatite and garnet end-members are from Ashley *et al.,* (2017) and Holland and Powell, (2011) respectively. Ashley *et al.,* (2017) provide isomekes diagrams for fluor- chlor- and hydroxylapatite inclusions hosted in almandine, pyrope, and andradite.

Analysis of Uncertainty

The stated instrumental uncertainty on the Thermo Nikolet Almega microRaman system that was used is ±0.1 cm^{-1}. This uncertainty associated with analysis and peak fitting corresponds to a *P* uncertainty of ±22 MPa based on a ~22 MPa/0.1 cm^{-1} shift.

To determine the maximum *P* uncertainty associated with the calculation of P_{inc} at room *T* according to the equation of Schouwink et al. (2010), we applied both the

maximum and minimum values of the regression parameters to our most pressurized apatite inclusion with the peak position of 965.605 cm^{-1}. This step adds only ~±0.04 MPa uncertainty, thus has little effect on estimating the P_{inc} at ambient *T* (25°C).

A linear mixing model was used to determine the physical properties of both our apatite inclusions and host garnet grains, based on the physical properties of their respective end-members. It is difficult to quantify the uncertainty associated with this assumption as it is not a given that the bulk modulus of our specific compositions of apatite and garnet will lie between the bulk modulus values of the mineral's respective end-members. The work regarding the calculation of the bulk moduli for these specific compositions of apatite ($F_{72}OH_{28}$) and garnet ($Adr_{90}Grs_{10}$) has yet to be performed, but would contribute to a more precise elastic model.

The uncertainty associated with the mineral equilibrium *P*-*T* estimates performed by Harris and Einaudi (1982) was not reported. Kohn and Spear (1990) reported that the uncertainty associated with mineral equilibrium thermobarometry under these conditions is typically ca. ±10 MPa and ±10°C, which would not significantly affect the *P*- or *T*-ranges of our model.

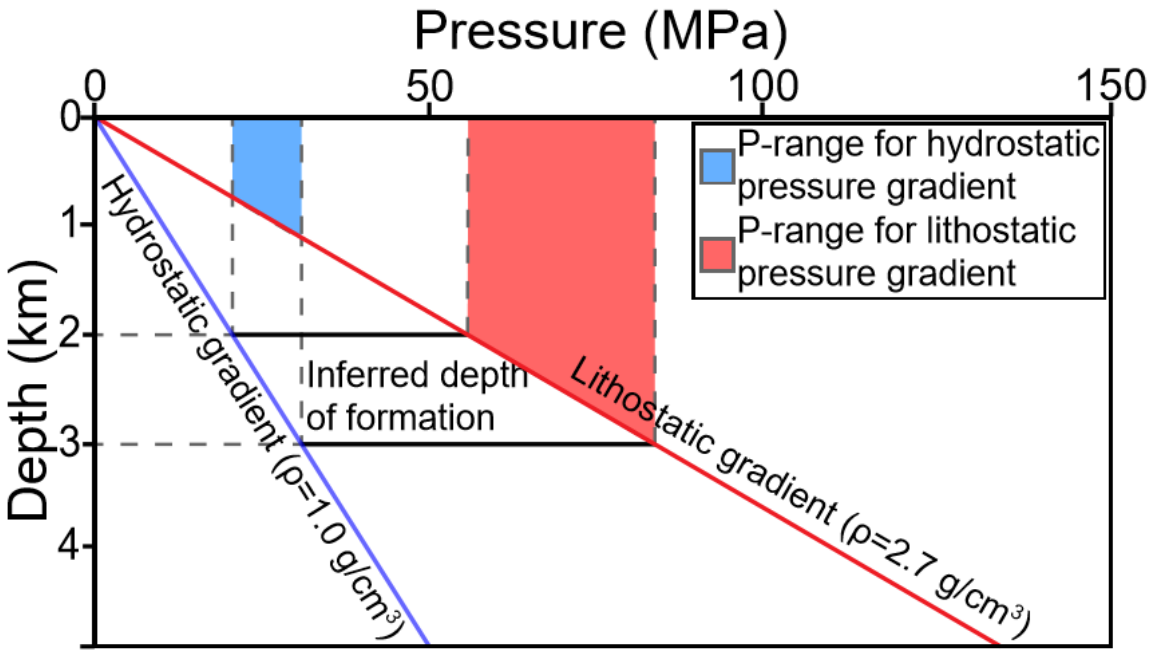

Figure DR1. - Figure detailing the differences in formation *P* as a function of depth within shallowly emplaced hydrothermal systems. At greater depths, the lithostatic *P* gradient controls the system but due to its shallow formation depth, the Casting Copper skarn likely formed at *P* between the two extremes represented by each of these *P* gradient end-members.

Table DR1. - Normalized major element compositional data of Casting Copper garnets determined using an electron microprobe (EPMA). For consistency, the garnet was treated as an average composition of $Adr_{90}Grs_{10}$. Sensitivity analyses show that the calculated formation *P* differences for the extremes of grossular composition were on the order of ±32 MPa for the extremes of grossular content.

Sample	Si(T)	P(T)	Al(T)	Fe^{3+}(T)	Σ(T)	Al(6)	Fe^{3+}(6)	Mn^{3+}(6)	Σ(6)	Ca(8)	Fe^{2+}(8)	Mg(8)	Mn^{2+}(8)	Na(8)	K(8)	Σ(8)
CC04-01	2.986	0.003	0.011	0.000	3.00	0.054	1.942	0.000	2.00	2.985	0.009	0.002	0.006	0.000	0.000	3.00
CC01-05	2.966	0.002	0.031	0.000	2.99	0.070	1.910	0.003	1.98	3.013	0.000	0.001	0.000	0.001	0.001	3.02
CC01-02	2.965	0.003	0.031	0.000	2.99	0.073	1.910	0.007	1.99	3.009	0.000	0.000	0.000	0.000	0.000	3.01
CC03-01	2.966	0.003	0.031	0.000	3.00	0.087	1.897	0.007	1.99	3.006	0.000	0.001	0.000	0.000	0.001	3.01
CC03-06	2.975	0.003	0.021	0.000	2.99	0.110	1.884	0.000	1.99	2.997	0.006	0.002	0.001	0.000	0.000	3.01
CC01-03	2.985	0.003	0.012	0.000	3.00	0.251	1.740	0.000	1.99	2.995	0.004	0.000	0.007	0.003	0.000	3.01
CC03-05	2.990	0.003	0.007	0.000	3.00	0.222	1.772	0.000	2.00	2.995	0.004	0.002	0.005	0.000	0.000	3.00

CC01-06	2.964	0.003	0.034	0.000	3.00	0.337	1.648	0.005	1.99	3.005	0.000	0.003	0.000	0.002	0.000	3.01
CC01-04	2.963	0.003	0.034	0.000	3.00	0.476	1.519	0.005	2.00	2.997	0.000	0.000	0.000	0.002	0.000	3.00
CC01-07	2.975	0.003	0.022	0.000	3.00	0.696	1.316	0.005	2.02	2.980	0.000	0.000	0.001	0.000	0.000	2.98

75

76 Table DR2. - Sample ID's with their coordinate locations and sample descriptions.

Sample ID	Location Lat (°N) Long(°W)	Notes
CC01	38°56'44.7" 119°16'24.5"	Several apatite inclusions at depth, suitable for mineral inclusion analysis
CC02	38°56'44.7" 119°16'24.5"	Abundant apatite + calcite inclusions, apatite exposed at surface, suitable for mineral inclusion analysis
CC03	38°56'44.6" 119°16'23.2"	Abundant apatite + calcite inclusions, two apatites exposed at surface, prevalent zonations in garnet with apatite inclusions across them, suitable for mineral inclusion analysis
CC04	38°56'44.6" 119°16'23.2"	Few inclusions of apatite + hematite, prevalent zonations in garnet, relict calcite grains, not suitable for fluid inclusion analysis
CC05	38°56'44.6" 119°16'23.2"	Prevalent zonations, only one apatite inclusion present near crack, not suitable for mineral inclusion analysis
CC06	38°56'44.9" 119°16'24.9"	No apatite inclusions present, not suitable for mineral inclusion analysis
CC07	38°56'44.9" 119°16'24.9"	No apatite inclusions present, not suitable for mineral inclusion analysis
CC08	38°56'46.5" 119°16'25.3"	Abundant apatite inclusions at depth and two at the surface, several inclusions located near cracks, contains clusters of apatite inclusions and relict calcite grains, suitable for mineral inclusion analysis
CC09	38°56'46.5" 119°16'25.3"	Few inclusions of apatite + hematite, prevalent zonations in garnet, suitable for mineral inclusion analysis
CC10	38°56'44.4" 119°16'25.5"	Several apatite inclusions, two located near cracks/ sample surface, suitable for mineral inclusion analysis
CC11	38°56'44.4" 119°16'25.5	No apatite inclusions but contains both ilmenite and hematite inclusions, not suitable for mineral inclusion analysis
CC12	38°56'44.4" 119°16'25.5"	No apatite inclusions present, not suitable for mineral inclusion analysis
CC13	38°56'44.4" 119°16'25.5"	Two apatite inclusions, one located near surface, not suitable for mineral inclusion analysis
CC14	38°56'45.2" 119°16'25.5"	Several apatite and hematite inclusions, prevalent zonations, suitable for mineral inclusion analysis
CC15	38°56'45.2" 119°16'25.5"	No apatite inclusions present, not suitable for mineral inclusion analysis
CC16	38°56'45.2" 119°16'25.5"	Several apatite + calcite inclusions, apatites located near cracks/ sample surface, suitable for mineral inclusion analysis

Table DR3. - Normalized major element compositional data of apatite inclusions contained within Casting Copper garnets determined using an electron microprobe (EPMA). Fluorapatite is the most compressible (lowest bulk modulus) variety of apatite, followed closely by hydroxylapatite; chlorapatite shows a more marked difference in bulk modulus compared to F-OH apatite (e.g., Matsukage *et al.,* 2004) Although there is some variability in composition between apatite inclusions, because there is such a slight difference between the bulk moduli of fluor- and hydroxylapatite, we treated the apatites as an average composition of $F_{72}OH_{28}$ because our results are not much affected by the compressibility of chlorapatite or non-ideal mixing between end-members.

Sample	Ca(A)	Fe^{2+}(A)	Σ(A)	P(T)	Si(T)	S(T)	Σ(T)	F(H)	Cl(H)	OH(H)	Σ(H)
CC1-01-05	5.049	0.028	5.077	2.908	0.003	0.003	2.915	0.736	0.031	0.234	1.000
CC1-04-02	5.200	0.013	5.213	2.770	0.009	0.000	2.778	0.957	0.043	0.000	1.000
CC1-02-04	4.991	0.027	5.019	2.965	0.006	0.000	2.971	0.615	0.001	0.384	1.000
CC1-01-01	5.058	0.010	5.068	2.905	0.017	0.001	2.925	0.667	0.023	0.310	1.000
CC1-02-01	5.075	0.019	5.094	2.877	0.020	0.001	2.897	0.721	0.005	0.274	1.000
CC1-03-05	5.017	0.022	5.040	2.947	0.006	0.001	2.956	0.553	0.000	0.447	1.000
CC1-04-01	5.045	0.012	5.057	2.909	0.024	0.001	2.934	0.503	0.005	0.492	1.000
CC1-01-02	5.062	0.019	5.080	2.891	0.018	0.001	2.911	0.806	0.007	0.187	1.000
CC1-01-03	5.059	0.021	5.080	2.889	0.020	0.003	2.912	0.705	0.011	0.285	1.000
CC1-03-02	5.044	0.028	5.072	2.915	0.007	0.002	2.925	0.859	0.001	0.141	1.000
CC1-02-03	5.039	0.025	5.064	2.920	0.005	0.002	2.927	0.724	0.000	0.276	1.000
CC1-01-07	5.076	0.022	5.097	2.882	0.016	0.000	2.898	0.642	0.049	0.309	1.000
CC1-01-04	5.026	0.027	5.052	2.920	0.016	0.001	2.938	0.805	0.066	0.129	1.000
CC1-03-01	5.031	0.020	5.051	2.921	0.018	0.000	2.941	0.642	0.002	0.356	1.000
CC1-03-04	5.027	0.016	5.043	2.927	0.017	0.001	2.945	0.652	0.051	0.298	1.000
CC1-03-03	5.010	0.036	5.046	2.927	0.018	0.001	2.946	0.730	0.001	0.269	1.000
CC1-02-02	5.012	0.021	5.033	2.942	0.018	0.000	2.960	0.866	0.003	0.131	1.000

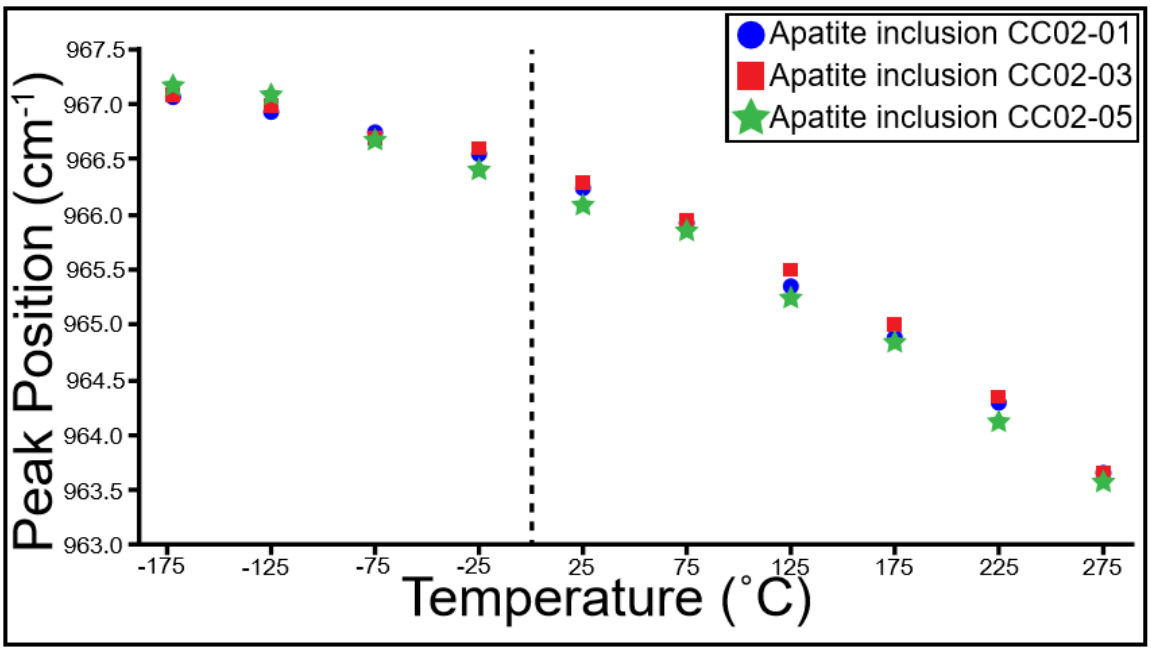

Figure DR2. - Figure detailing the T-dependent wave shift of apatite inclusions at ambient *P*. As *T* increases, bond lengths increase as well, leading to a lower Raman peak position.

Table DR4. Inclusion IDs and their respective peak positions, Δpeak, P_{inc} at 25°C, P_{form} at 400°C. Uncertainties are based on the standard deviation of measured peak positions (replicates) of a Durango apatite standard. Bolded entries represent samples that are exposed at the sample surface while samples that are located near a crack or the surface and have lost *P* are italicized.– Raman peak position uncertainties determined using standard deviation.– Raman peak position of apatite standard exposed at surface of the garnet containing no internal *P*.

Sample ID	Raman peak position (cm^{-1})	Standard peak position (cm^{-1})	Δ_{peak} (cm^{-1})[a]	P_{inc} @ 25°C (MPa)[b]	P_{inc} uncertainty @ 25 °C (MPa)	$P_{form.}$@ 400°C (MPa)[c]	P_{form} uncertainty @ 400°C (MPa)[d]
CC01-01	965.919	966.318	-.399	-89.4	±22	7.0	±22
CC01-02	965.939	966.318	-.379	-84.9	±22	22.8	±22

CC01-03	965.979	966.318	-.339	-75.9	±22	54.9	±22
CC01-04	965.869	966.318	-.449	-100.6	±22	-32.7	±22
CC02-01	965.885	966.318	-.433	-97.0	±22	-20.3	±22
CC02-02	965.905	966.318	-.413	-92.5	±22	-4.4	±22
CC02-03	966.115	966.318	-.203	-45.5	±22	164.2	±22
CC02-04	965.985	966.318	-.333	-74.6	±22	59.4	±22
CC02 inc-1	**966.323**	**966.318**	**.005**	**1.1**			
CC02 inc-2	965.933	966.318	-.385	-86.2	±22	17.9	±22
CC02 inc-3	966.043	966.318	-.275	-61.6	±22	105.9	±22
CC02 inc-4	*966.273*	*966.318*	*-.045*	*-10.1*			
CC02 inc-5	965.883	966.318	-.435	-97.4	±22	-21.8	±22
CC02 inc-6	966.073	966.318	-.245	-54.9	±22	130.1	±22
CC02 inc-7	966.003	966.318	-.315	-70.6	±22	74.2	±22
CC03 sur.	**966.285**	**966.318**	**-.033**	**-7.4**			
CC03 sur-2	**966.305**	**966.318**	**-.013**	**-2.9**			
CC03-02	965.935	966.318	-.383	-85.8	±22	19.8	±22
CC03-03	965.905	966.318	-.413	-92.5	±22	-4.4	±22
CC03-04	965.945	966.318	-.373	-83.5	±22	27.7	±22
CC03-05	966.075	966.318	-.243	-54.4	±22	132.1	±22
CC03-06	965.025	966.318	-.293	-65.6	±22	91.5	±22
CC03-07	966.045	966.318	-.273	-61.1	±22	107.8	±22
CC08-01	**966.325**	**966.318**	**.007**	**1.6**			
CC08-02	*966.245*	*966.318*	*-.073*	*-16.4*			
CC08-03	*966.325*	*966.318*	*.007*	*1.6*			
CC08-04	965.945	966.318	-.373	-83.6	±22	27.7	±22
CC08-05	966.035	966.318	-.283	-63.4	±22	99.5	±22
CC08-06	965.935	966.318	-.383	-85.8	±22	19.8	±22
CC08-07	966.025	966.318	-.293	-65.6	±22	91.5	±22
CC08 inc-1	*966.36*	*966.318*	*.042*	*9.4*			
CC08 inc-2	965.99	966.318	-.328	-73.5	±22	63.8	±22
CC08 inc-3	**966.35**	**966.318**	**.032**	**7.2**			
CC09-01	*966.203*	*966.318*	*-.115*	*-25.8*			
CC09-02	966.003	966.318	-.315	-70.6	±22	74.2	±22
CC10-01	*966.275*	*966.318*	*-.043*	*-9.6*			
CC10-02	966.075	966.318	-.243	-54.4	±22	132.1	±22
CC10-03	*966.365*	*966.318*	*.047*	*-10.5*			
CC10-04	966.033	966.318	-.285	63.4	±22	98.0	±22
CC13-01	966.008	966.318	-.310	-69.4	±22	78.2	±22
CC13-02	*966.298*	*966.318*	*-.002*	*-4.5*			
CC14-01	*966.435*	*966.318*	*-.117*	*26.2*			
CC14-02	965.955	966.318	-.363	-81.3	±22	35.6	±22
CC14-03	966.025	966.318	-.293	-65.6	±22	91.5	±22
CC14-04	965.985	966.318	-.333	-74.6	±22	59.4	±22
CC15-01	*966.220*	*966.318*	*-.098*	*-22.0*			
CC16-01	966.024	966.318	-.294	-65.9	±22	91.0	±22
CC16-02	*966.275*	*966.318*	*-.043*	*-9.6*			

CC16-03	*966.245*	*966.318*	*-.073*	*-16.4*			
CC16-04	*966.305*	*966.318*	*-.013*	*-2.9*			
CC16-05	966.105	966.318	-.213	-47.7	±22	156.3	±22

(a) – The difference between the peak position of the apatite standard and the apatite inclusion.

(b) – Internal *P* of inclusions at 25°C calculated from Δ_{peak} using the equation of Comodi et al. 2001 ($P_{inc}=(\frac{Vp}{Vo}-1)/\beta$ where ν_o is the standard peak position, ν_o is the inclusion peak position, and $\beta = 0.00462$ for apatite.

(c) – Formation *P* of inclusions at 400°C calculated from Δ_{peak} using the elastic model of Guiraud and Powell, (2006).

(d) *P* uncertainty of elastic model based on Raman peak position uncertainties.

REFERENCES CITED IN SUPPLEMENTAL FIGURES

Ashley, K.T., Barkoff, D.W., and Steele-MacInnis, M., 2017, Barometric constraints based on apatite inclusions in garnet: American Mineralogist, v. 102, DOI: http://dx.doi.org/10.2138/am-2017-5898.

Babuska, V., Fiala, J., Kumazawa, M., and Ohno, I., 1978, Elastic properties of garnet solid-solution series: Physics of the Earth and Planetary Interiors, v. 16, p. 157-176, doi:10.1016/0031-9201(78)90086-9.

Guiraud, M., Powell, R., 2006, P-V-T relationships and mineral equilibria in inclusions in minerals: Earth and Planetary Science Letters, v. 244, p. 683-694, doi:10.1016/j.epsl.2006.02.021.

Holland, T.J.B., and Powell, R., 2011, An improved and extended internally consistent thermodynamic dataset for phases of petrological interest, involving a new equation of state for solids: Journal of Metamorphic Geology, v.29(3), p. 333-383, doi:10.1111/j.1525-1314.2010.00923.x.

Kohn, M.J., and Spear, F.S., 1990, Two new geobarometers for garnet amphibolites, with applications to southeastern Vermont: American Mineralogist v. 75, p. 89-96.

Matsukage, K.N., Ono, S., Kawamoto, T., and Kikegawa, T., 2004, The compressibility of natural apatite: Physics and Chemistry of Minerals, v. 31(9), p. 580-584, doi:10.1007/s00269-004-0415-x.

Robie, R.A., Hemingway, B.S., and Fisher, J.R., 1978, Thermodynamic properties of minerals and related substances at 298.15 K and 1 bar (10/sup 5/pascals) pressure and at higher temperatures: USGS Bulletin – 1452.

Schouwink, P., Miletich, R., Ullrich, A., Glasmacher, U. A., Trautmann, C., Neumann, R., and Kohn, B. P., 2010, Ion tracks in apatite at high pressures: the effect of crystallographic track orientation on the elastic properties of fluorapatite under hydrostatic compression: Physics and Chemistry of Minerals, v. 37(6), p. 371-387, doi:10.1007/s00269-009-0340-0.